Plateau Reactions: Double Proton-Transfer Processes with Structureless Transition States

Stefan Schweiger and Guntram Rauhut*

Institut für Theoretische Chemie, Universität Stuttgart, Pfaffenwaldring 55, 70569 Stuttgart, Germany

Received: April 15, 2003; In Final Form: August 1, 2003

The double proton-transfer reactions of the model base pair systems pyrazole−pyrazole and pyrazole−guanidine have been studied by computational methods up to the CCSD(T)/aug-cc-pVTZ level. In contrast to the synchronous proton transfer of the pyrazole dimer, the reaction profile of the second system shows a plateaulike transition region instead of a well-defined transition state characterized by one structure on the energy hypersurface. According to the computational results of this study, such plateau reactions with structureless transition regions behave differently in comparison to standard systems with gauss-shaped barriers. Energy partitioning schemes were used to analyze the unusual reaction profile, and one-dimensional tunneling effects were accounted for by a numerical approach. An empirical scheme has been derived to predict plateau reactions for double proton transfer systems.

1. Introduction

The common understanding of an elementary chemical process refers to a set of reactants, a well-defined transition state being higher in energy than the reactants, and the products of the reaction. More complicated reactions usually consist of consecutive series of such processes and thus involve reactive intermediates. Other classes of chemical processes, as for example homolytic bond dissociations, may differ from that scheme and do not require the existence of a transition state. For those reactions that do involve a transition state, the question arises whether a transition state is always a well-defined (stationary) point on the potential energy surface (PES). Generalizations of this simple concept, which is based on a static point of view, to structureless transition regions, in which the transition state cannot be described by just one point on the PES, appear feasible. In the case of such reactions, far-reaching consequences must be anticipated, but the foremost aspect certainly concerns the occurrence of such processes.

Within this context, the study presented in this paper focuses on the principal investigation of double proton transfer reactions (DPTR) based on quantum chemical calculations. DPTRs are of utmost importance for biochemical processes and thus life sciences in general. Many experimental and computational studies focus on the relative stabilities,[1] frequency shifts,[2,3] etc., of molecular clusters in which two monomers are linked by two hydrogen bonds. The most prominent examples in that respect constitute the clusters of nucleic acid base pairs (e.g., adenine−thymine).[4] The investigation of such clusters by means of quantum chemical calculations is hindered by several aspects: (1) the size of the system, (2) many local minima on the PES, (3) long-range effects (dispersion contributions to the interaction energy) that cannot be accounted for at the RHF (restricted Hartree−Fock) or DFT (density functional theory) level, and (4) the need for large basis sets for a proper treatment of the intermolecular interactions. The investigation of reaction barriers of DPTRs becomes even more tedious since tunneling corrections need to be considered, and a proper treatment certainly requires dynamics calculations to be performed.[5]

* To whom correspondence should be addressed: rauhut@theochem.uni-stuttgart.de.

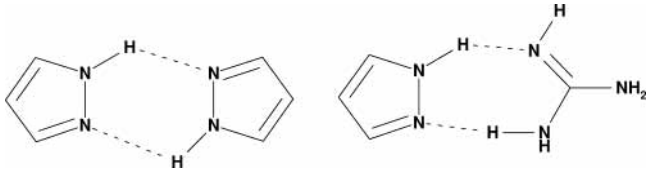

Figure 1. Pyrazole−pyrazole and pyrazole−guanidine model clusters.

Due to the computational problems outlined above, we did not focus on base pairs themselves but rather on model systems consisting of (a) two pyrazole units or (b) one pyrazole entity and a guanidine molecule (cf. Figure 1). Besides serving as models of the biochemical systems, these clusters constitute a highly interesting chemical system in itself. The advantages of using these species are as follows: (1) they are significantly smaller and thus more accurate computational methods can be used, (2) fewer local minima allow for fewer possible reaction mechanisms, and finally (3) symmetry can be exploited within the investigation of the reaction paths. Throughout this paper we compare the results obtained for both systems.

DPTRs have extensively been studied by experimental and computational approaches. In particular, Limbach and co-workers[6,7] studied kinetic isotope effects using dynamic NMR spectroscopy. Besides other systems, they focused on multiple proton transfers in solid pyrazole derivatives. Most relevant for the study presented here is the combined experimental and computational work of de Paz et al.[8] about the proton transfers in the pyrazole dimer and higher oligomers. Comparison to the experimental results presented in this study will be made wherever possible. Other computational studies concern dimers of carboxylic acids,[5] model base pairs,[9] the formamide dimer,[10,11] and many other systems.[12−14] The main question tackled in these papers concerns the nature of the proton transition, i.e., a concerted or successive process. Peeters et al.[15] computed the proton affinities of guanidine and related systems at the MP2/6-31G(d,p) level.

The paper is structured as follows: section 2 summarizes the computational methods used within the calculations. Section 3 focuses on the investigation of the minimum energy reaction paths (MEP) and the energy partitioning with respect to selected internal coordinates. Solvent effects on the reaction profiles

10.1021/jp0350060 CCC: $25.00
Published on Web 10/18/2003

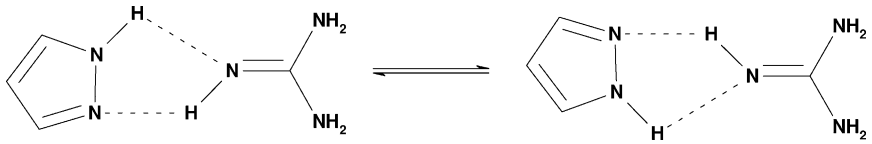

Figure 2. Alternative reaction path via a five-membered ring system.

and effects due to substituents are discussed in section 4. Vibrational corrections and tunneling effects are considered in sections 5 and 6, respectively, and an attempt for the prediction of DPTRs with structureless transition regions is made in section 7.

2. Computational Details

All geometries were determined at the MP2/[aug]-cc-pVDZ level.[16] The augmented diffuse functions, i.e., [aug], are enclosed in brackets since they have been added to the four heavy atoms and the two hydrogens involved in the N···H hydrogen bonds of the clusters only. Likewise, frequency calculations were performed at the same level of theory. Relative energies were determined at the CCSD(T)/[aug]-cc-pVDZ level[17] or the MP2/[aug]-cc-pVDZ level,[18] respectively. Since the [aug]-cc-pVDZ basis set must be considered small in comparison to the level of the electronic structure calculations, its reliability for the systems of this study has been checked against the results of CCSD(T)/[aug]-cc-pVTZ calculations for some symmetrical clusters. All quantum chemical calculations have been performed with the MOLPRO,[19] GAMESS-US,[20] and GAUSSIAN98[21] program packages. The intrinsic reaction coordinates (IRC) have been traced by the Gonzalez−Schlegel algorithm[22,23] with a step width of 0.05 amu$^{1/2}$·Bohr. If not otherwise noted, the reaction coordinates used in this study refer to mass-weighted coordinates. However, in several cases it was necessary to switch to simple distance coordinates without mass weighting. All energy profiles presented here refer to fully relaxed structures, i.e., no constraints have been imposed on any of the structures. The conductorlike screening model (COSMO) as implemented in GAMESS-US was used for solvent simulations at the self-consistent reaction field (SCRF) level.[24] The dielectric constant has been varied in the range between 2.0 and 20.0 in order to simulate solvents of different polarity. Since continuum models are not able to handle specific solvent effects, we consider the results obtained by this approach qualitatively rather than quantitatively. For variational transition-state theory (VTST) calculations[25,26] the POLYRATE program[27] was used. The minimum energy paths (MEP) of the reactions were interpolated from the geometries, gradients, and Hessian information of the stationary points plus series of additional points on each side of the transition state from interpolated VTST by mapping (IVTST-M).[28] Interaction energies were corrected for basis-set superposition errors (BSSE) by the counterpoise correction scheme of Boys and Bernardi.[29] However, within this scheme, geometry relaxation contributions were neglected for the same reasons as discussed in detail recently.[30]

3. Intrinsic Reaction Coordinates

As found recently within the investigation of the proton-transfer mechanisms in 1,2,3-triazoles,[30] the intramolecular proton transfer in pyrazoles is energetically significantly less favorable than an autocatalytic mechanism via a second pyrazole entity or a different catalyst. For that reason, this mechanism will not be considered in further detail. In the following, the autocatalytic self-exchange reaction will be denoted reaction A and the guanidine-assisted DPTR will be called reaction B. Reaction B allows for two alternative pathways in principle, one of them being characterized by a five-membered (cf. Figure 2) ring system between the two molecules and the other being characterized by a seven-membered ring (cf. Figure 1). According to calculations at the MP2/[aug]-cc-pVDZ level, the reaction path via the five-membered ring has an activation energy 59.1 kJ/mol higher than the other. Therefore, the reaction path with the five-membered ring moiety will not be considered in further detail, and thus reaction B denotes the path of the cluster showing a seven-membered ring system. Activation energies for reaction paths A and B are listed in Table 1. The activation energy computed for reaction A is significantly lower than the value reported by de Paz et al.[8] (i.e., 122.2 kJ/mol at the SCF level). We attribute this discrepancy to the different computational levels. However, this comparison demonstrates the importance of high-level correlation effects for these proton transfers. The results in Table 1 indicate that MP2 tends to underestimate the reaction barriers by 10−15 kJ/mol, while the size of the basis set appears to be less crucial: for reaction A the [aug]-cc-pVTZ result differs from the [aug]-cc-pVDZ activation barrier by just 0.9 kJ/mol. For that reason the [aug]-cc-pVDZ basis has been used for all calculations. Reaction B is favored over path A by 26.0 kJ/mol at the CCSD(T)/[aug]-cc-pVDZ level. This effect can be rationalized on the basis that guanidine is a better proton acceptor than pyrazole. The most important geometrical N−H parameters of the complexes involved in the mechanisms are summarized in Table 2. These atomic distances show that in the reactants of reaction B one hydrogen bond is significantly shorter than the other. Consequently, one would not anticipate a synchronous proton transfer

TABLE 1: Activation Energies for the Autocatalytic Proton Transfer (A) and the Guanidine-Assisted Reaction (B)[a]

reaction	ΔE_{rel}[MP2] [aug]-cc-pVDZ	ΔE_{rel}[CCSD(T)] [aug]-cc-pVDZ	ΔE_{rel}[CCSD(T)] [aug]-cc-pVTZ	ΔZPE
A	45.8	61.2	62.1	24.1
B	25.4	35.2		14.2

[a] All values are corrected for the zero-point vibrational energies and are given in kilojoules per mole.

TABLE 2: Most Important Geometrical Parameters of the Reactants and Transition States of Reactions A and B Obtained from MP2/[aug]-cc-pVDZ Calculations[a]

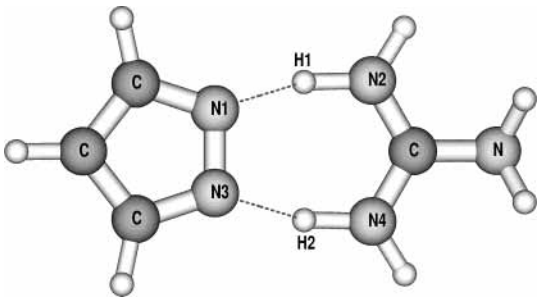

system	$r(N_1–H_1)$	$r(N_2\cdots H_1)$	$r(N_3\cdots H_2)$	$r(N_4–H_2)$
reactants of A	1.031	1.944	1.944	1.031
reactants of B	1.046	1.789	1.974	1.028
transition state of A	1.287	1.287	1.287	1.287
transition state of B	1.528	1.114	1.528	1.114

[a] Labeling of the atoms is provided for the transition state of reaction B. All parameters are given in angstroms.

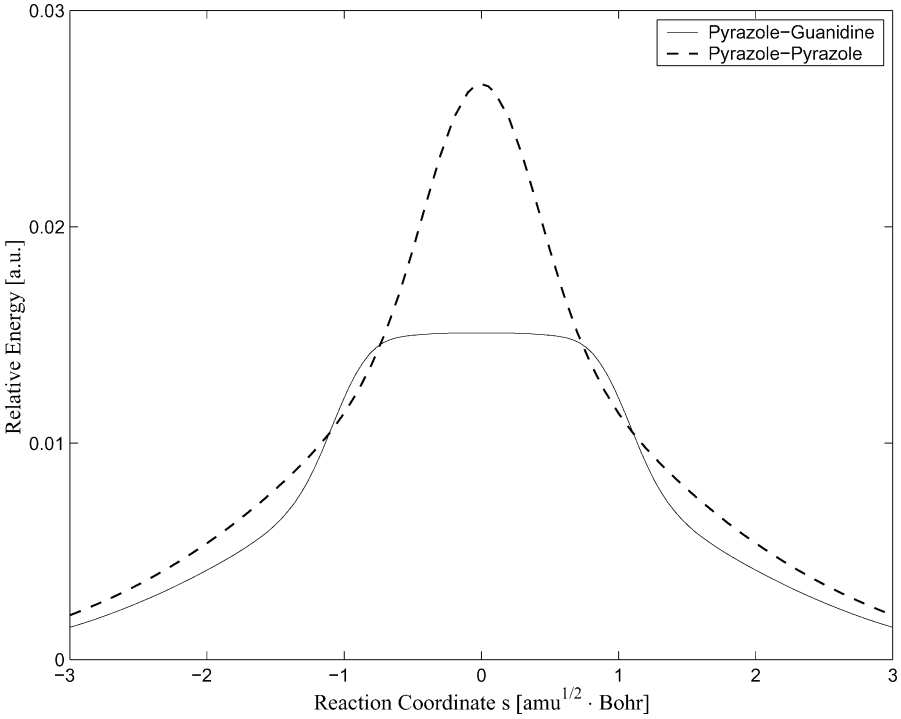

Figure 3. Reaction profiles of reactions A and B at the MP2 level.

for this system. This is supported by the geometrical parameters of the transition states: while all four atom distances are identical for reaction A, the transition state of reaction B is zwitterionic in nature, i.e., both protons reside very close to the guanidine entity. These results are in agreement with those of de Paz et al.,[8] who found a synchronous mechanism for reaction A as long as constraints were not imposed on the structures.

The most interesting aspect concerns the energy profiles of these two reactions, displayed in Figure 3. While the autocatalytic reaction A is characterized by a typical Eckart potential,[31] the guanidine-assisted DPTR shows a plateaulike transition region rather than a well-defined transition state. Within a range of about 1.0 amu$^{1/2}$•Bohr, the potential energy remains almost constant ($\Delta E \sim 0.3$ kJ/mol). Consequently, from a physical point of view the transition state of reaction B is structureless and thus each point on the plateau nearly fulfills the mathematical requirements for a transition state. The flat transition region results in dramatically lower imaginary frequencies for the plateau reaction than for the autocatalytic process: i.e., -132 cm^{-1} vs -1468 cm^{-1}. Moreover, it is anticipated that the shape of the potential must have significant impact on the physical properties of the reaction, as for example the transmission probability (vide infra). Since the potentials shown in Figure 3 were computed at the MP2/[aug]-cc-pVDZ level, which was found to underestimate the activation barriers by about 25%, the profile of the plateau reaction B was recomputed at the CCSD(T)/[aug]-cc-pVDZ level (i.e., energy single-point calculations on top of the MP2 geometries; cf. Figure 4). It is seen that the MP2 calculations predict the shape of the potential correctly but fail to provide accurate absolute values for relative energies. As a consequence, all further energy considerations refer to CCSD(T) calculations, while quantities relying on gradient information are based on MP2 results.

To understand the unusual profile of the plateau reaction, the profile was split into two fundamental contributions, each of them representing a potential closely related to the potential of a single proton transfer reaction (SPTR) step. Therefore, an energy partitioning scheme based on internal coordinates has been derived. The total differential dV(s) of the potential at any point of the reaction path s is given as

$$\mathrm{d}V(s) = \sum_{i=1}^{3N-6} \left(\frac{\partial V}{\partial q_i}\right) \mathrm{d}q_i \tag{1}$$

where the expression in parentheses denotes the energy gradients in internal coordinates q_i. Integration of this equation along the reaction path yields

$$V(s) = \sum_{i=1}^{3N-6} \int_{q_i(s_R)}^{q_i(s)} \left(\frac{\partial V}{\partial q_i}\right) \mathrm{d}q_i \tag{2}$$

where $q_i(s_R)$ denotes the value of an internal coordinate q_i at the geometry of the reactants. The summation in eq 2 can be split into n_{frags} chemical meaningful fragments F:

$$V(s) = \sum_{F=1}^{n_{frags}} \sum_{i\in\{F\}} \int_{q_i(s_R)}^{q_i(s)} \left(\frac{\partial V}{\partial q_i}\right) \mathrm{d}q_i \tag{3}$$

and thus energy contributions to the reaction profile belonging to any set of internal coordinates can be determined. By use of the GAMESS suite of ab initio programs,[20] energy gradients in internal coordinates were computed at the MP2 level. The integral in eq 3 can be solved by standard numerical integration schemes.

The internal coordinates that will mainly contribute to the reaction profile are the two NH distances and the NHN angle of both hydrogen-bond entities, which mainly represent the two SPTR steps during the reaction. The energy contributions of these three coordinates to the profile along the reaction path are provided in Figure 5. Most remarkably, the NHN angle has certain impact on the energy profile although its variation must be considered to be very modest (less than 5°). Investigation of other internal coordinates indicates that these three coordinates should sufficiently describe the energy profile in the plateau

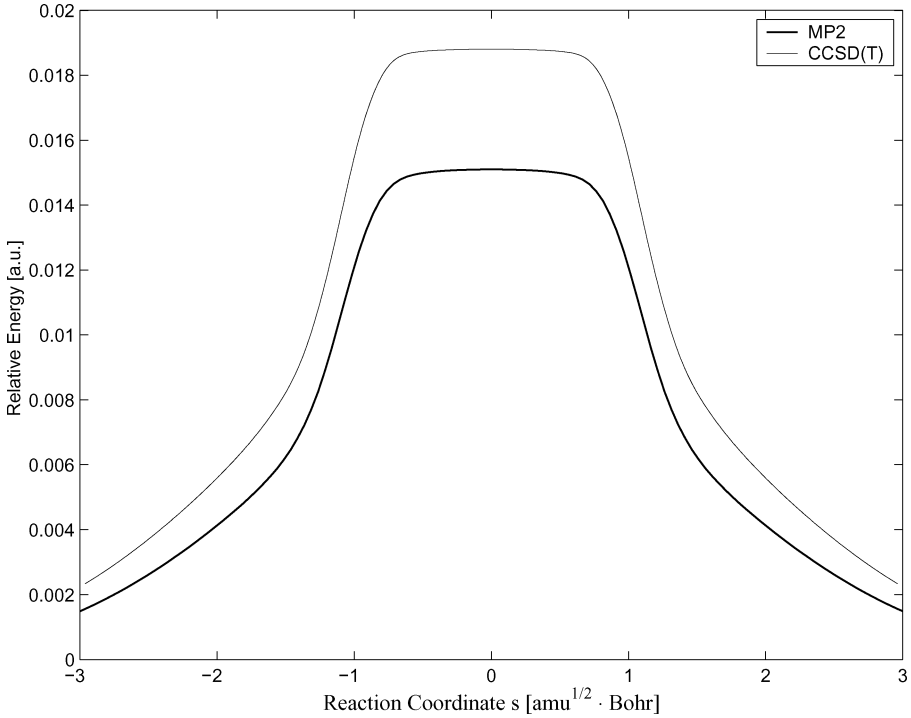

Figure 4. Comparison of the energy profiles of the plateau reaction at the MP2 and CCSD(T) levels.

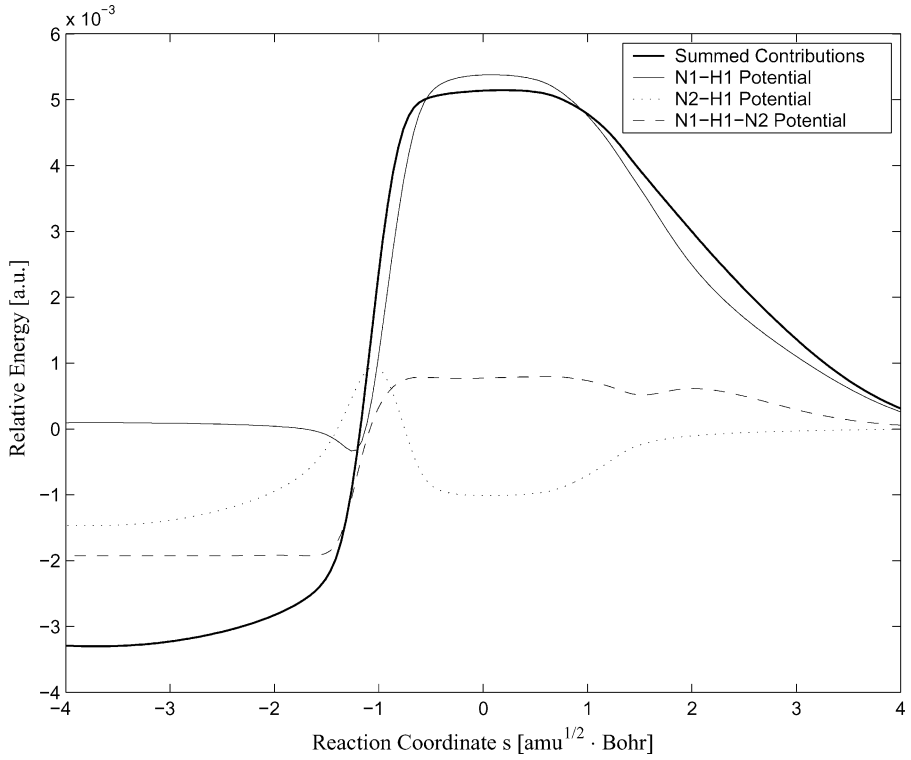

Figure 5. Energy contributions of selected internal coordinates to the reaction profile of mechanism B.

region. Therefore, three fragments *F* have been defined: the first two consist of the three internal coordinates belonging to each hydrogen bond, and the third fragment contains all other internal coordinates. As can be seen in Figure 6, summation of the first two fragments yields a proper description of the plateau and consequently, the total energy has successfully been split into the contributions of the two proton-transfer moieties. To allow for a better graphical comparison of the different potentials in Figure 6, constant offsets have been added to the curves of V_1, V_2, and V_{sum} that cause the potentials to converge toward zero at the structure of the reactants. In addition, the computed MP2 potential has been shifted in such a way that it coincides with V_{sum} at the transition state ($s = 0.0$). The shape of the energy profiles in Figure 6 was confirmed by a multidimensional Taylor expansion of the energy contributions based on gradient and frequency information in internal coordinates. However, due to the computationally demanding frequency calculations, we consider the approach via the total differential to be the preferable choice. Interestingly, the potentials of the single proton-transfer steps show a plateau region by themselves. We attribute this to electronic couplings between the two SPTRs, because the gradients used in eq 2 refer to the total energy of

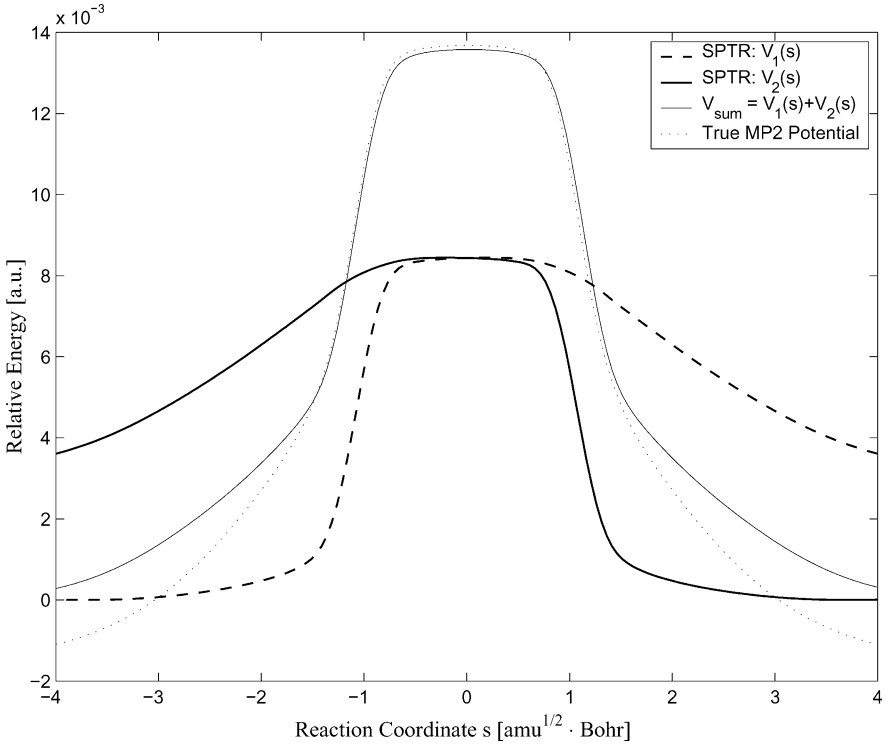

Figure 6. SPTR and DPTR potentials arising from subsets of internal coordinates in comparison to the true MP2 reaction profile.

the system rather than to the energy of the fragments. In other words, the SPTRs obtained from the procedure described above do not exactly represent a potential that arises from the transition of just one proton because energy contributions from the other proton transfer to the first one must be considered to be inherently absorbed. However, Figure 6 clearly demonstrates that the plateau results from a superposition of the two underlying SPTR potentials. Variation of the overlap of these two fundamental potentials will finally determine the nature of the reaction profile, i.e., gauss-shaped potential vs plateau reaction vs two separated gauss-shaped potentials with a zwitterionic intermediate in between. According to Figure 6, in the outer regions of the reaction (about $|s| > 1.5$ amu$^{1/2}$•Bohr) other coordinates dominate over those discussed above. In particular, we have focused on the relative position of the two molecules to each other. For that reason we have computed the centers of mass for both molecules within the cluster excluding the migrating protons. Figure 7 displays the distance between the centers of mass along the reaction coordinate. This plot indicates that in the first part of the reaction the intermolecular distance decreases while it remains almost constant during the DPTR.[32]

4. Impact of Solvents and Substituents

Due to the zwitterionic nature of the plateau region, substituents at the pyrazole entity and solvents will have a major impact on the reaction profile of reaction B. In order not to destroy the symmetry of the reaction profile, substituents have only been introduced in the C_4 position of the pyrazole molecule. Electron-withdrawing substituents will stabilize a zwitterionic reactive intermediate and will thus lead to a two-step mechanism, as could be shown recently for CN substituents in triazoles.[30] On the contrary, electron-donating substituents destabilize the system and will lead to higher activation barriers $\Delta E^{\ddagger}$ and thus may change the plateaulike potential toward an Eckart potential. In terms of the fundamental potentials of the SPTR steps, electron-donating substituents will lead to a stronger overlap, as could be confirmed by a series of calculations with different substituents. All these considerations can be rationalized on the basis of the Hammett relationships[33] in combination with classical transition-state theory according to

$$\Delta E^{\ddagger}_{X} = -[kT\rho \ln (10)]\sigma(T) + \Delta E^{\ddagger}_{\mathrm{H}} \qquad (4)$$

Herein $\sigma(T)$ denotes the Hammett parameter, T is the temperature, and X represents any substituent.[34] Of particular interest is the fluorine substituent. It leads to a slighty lower activation barrier of 22.0 kJ/mol at the MP2/[aug]-cc-pVDZ level and of 31.2 kJ/mol at the CCSD(T)/[aug]-cc-pVDZ level. This substituent does not destroy the plateau but leads to an even flatter transition region. For comparison (vide supra), within the range of 1.0 amu$^{1/2}$•Bohr the potential energy varies by about 0.07 kJ/mol. The potential of this reaction is provided in Figure 8. The imaginary frequency of the formal transition state is given by just -70 cm^{-1}. The plateau of the DPTR involving fluoropyrazole is also broader than that of the unsubstituted species. This effect had to be anticipated, since the two SPTR potentials will be shifted apart until they will be separated by a reactive intermediate in case of even stronger electron-withdrawing substituents.

The impact of solvent effects is closely related to that of substituents: polar solvents will stabilize a zwitterionic intermediate and will thus lead to two transition states. The influence of solvents has been studied by increasing the static dielectric constant within the continuum approach from 1.0 to 2.0, to 8.0, and finally to 20.0. Figure 9 shows the resulting shapes of the reaction potentials. The profiles presented in Figure 9 refer to COSMO calculations on top of the gas-phase geometries and thus, in a crude approximation, the reaction path is assumed not to alter due to solvent effects. The stabilization of the separated charges leads to a decrease of the overall activation barrier when the dielectric constant increases. Note that the width of the profile does not change significantly, while the central part alters dramatically. Consequently, the SPTR potentials are not shifted apart (as in the case of substituents) but the shape

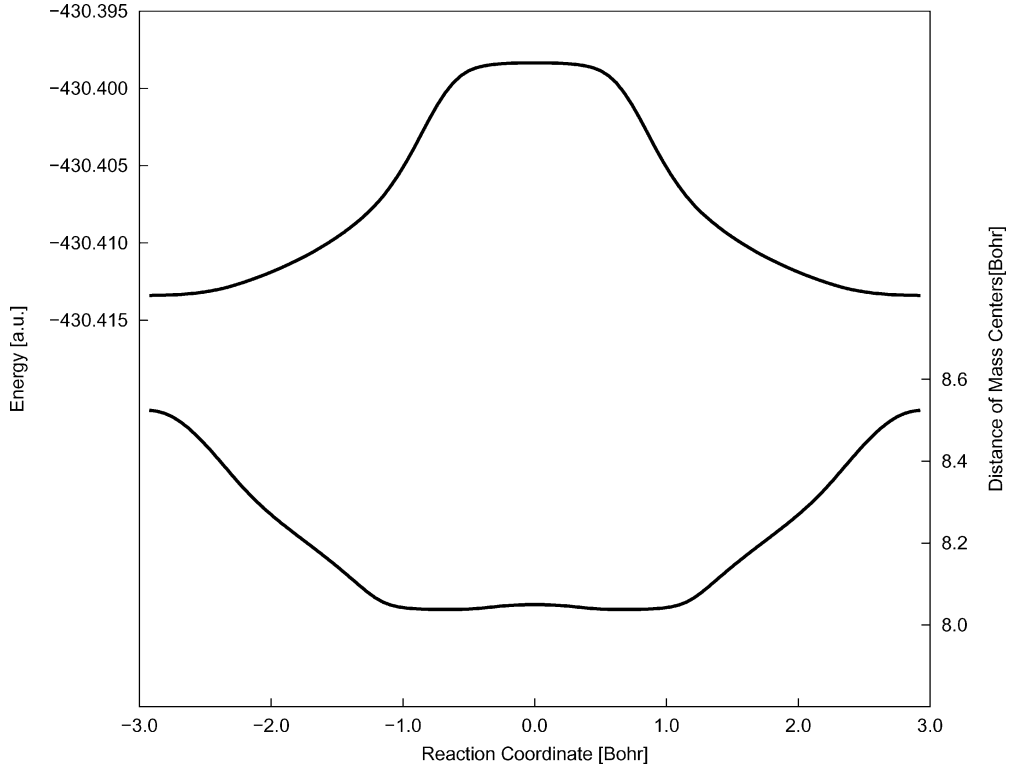

Figure 7. Distance of the centers of mass of the pyrazole and the guanidine entities plotted against the reaction coordinate.

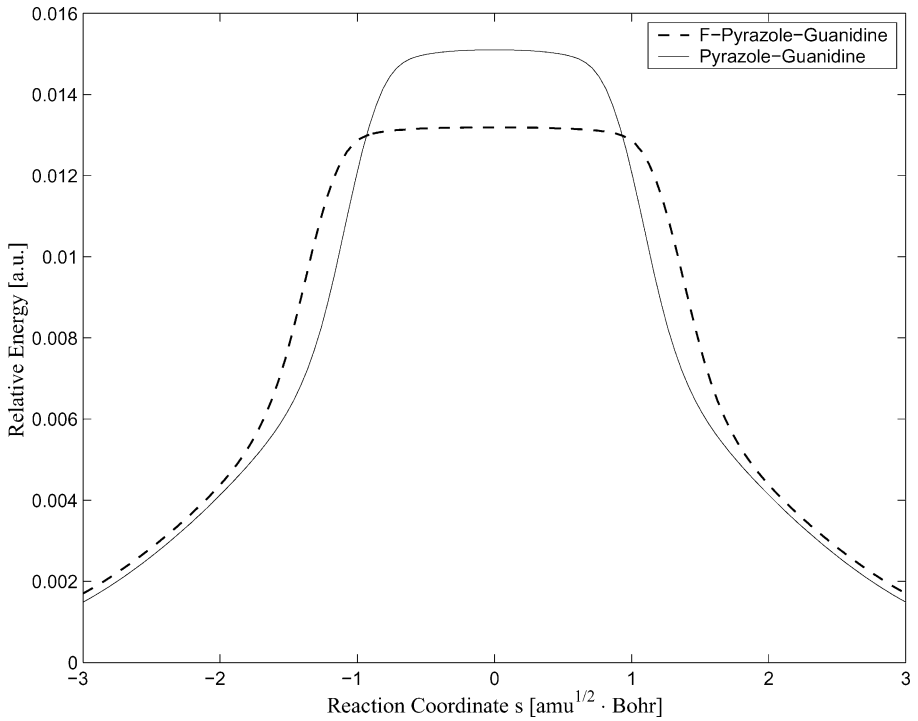

Figure 8. Comparison of the reaction profiles for the proton exchange between pyrazole and guanidine and fluoropyrazole and guanidine, respectively.

of the SPTR potentials changes and thus the coupling between them. However, this observation is restricted to the discussion when geometry relaxation effects have been neglected within the solvent simulation. Moreover, the continuum model used retains the symmetry of the reaction, which of course will not be the case in nature where specific solvent effects may lead to energy profiles very different than the presented one.

5. Vibrational Corrections

The energy profiles presented in Figure 3 refer to the potential energy without any corrections due to the vibrational levels of the molecules. The question arises whether zero-point vibrational energy corrections (ZPE) may alter the shape of the plateau reaction. A proper investigation of this aspect definitely requires dynamical calculations to be performed, which are currently in preparation. In a very crude approximation, one may consider ZPE corrections within the harmonic approximation by simply adding them to the total energy along the reaction path. Therefore, for estimating the impact of ZPE corrections we computed the ZPE along the reaction path for reaction B. To minimize the effects due to nonnegligible linear terms within

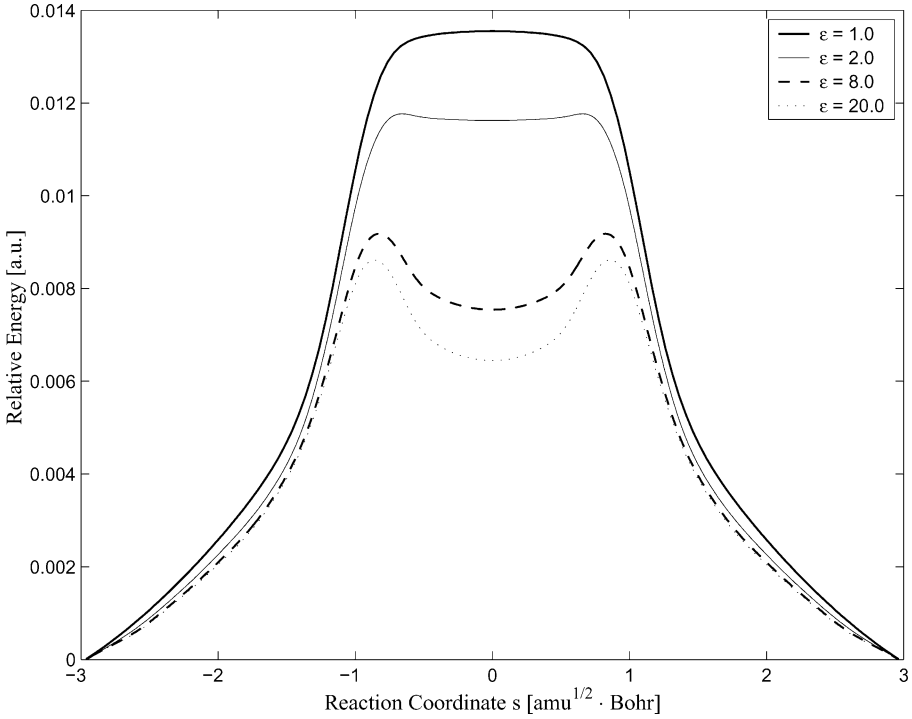

Figure 9. Impact on solvent effects on the energy profile of reaction B.

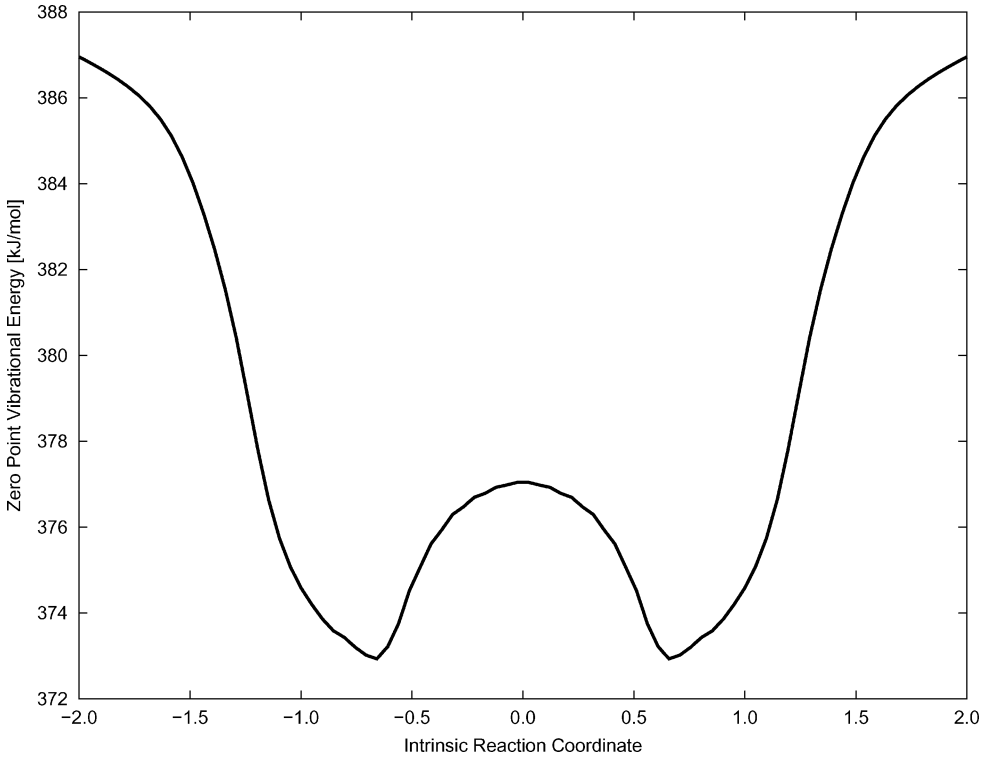

Figure 10. Zero-point vibrational energy along the reaction path of the plateau reaction.

the Taylor expansion of the potential, the projection scheme as described by Miller et al.[35] has been applied to all frequency calculations along the reaction path. According to this projection scheme, 7 frequencies will be projected out and all other modes are constrained to be orthogonal to the gradient vector. Moreover, the discussion will be restricted to the plateau region (i.e., -1.0 amu$^{1/2}$·Bohr $\leq s \leq$ 1.0 amu$^{1/2}$·Bohr), where the corrections due to the projection technique were found to be extremely small. The corresponding plot of the projected ZPE is provided in Figure 10. The ZPE reaches minima at the edges of the plateau and—in contrast to many other reactions—a local maximum at the formal transition state. According to this curve the ZPE is about 4.1 kJ/mol lower at the edges of the plateau (minima of the curve) than in the middle. This would formally destroy the plateau presented in Figure 3. Under the assumption that the shape of the ZPE correction is correct, it must be kept in mind that solvent effects and substituent effects act in the opposite direction and thus may effectively cancel out the ZPE correction (cf. Figure 9). For example, within the solvent simulation with $\epsilon = 8.0$ the zwitterionic intermediate is stabilized by about 4.2 kJ/mol with respect to the transition states and thus effectively compensates for the ZPE correction. Note that

in our previously studied system of 4-cyanotriazole and guanidine (see ref 30), which shows a zwitterionic intermediate, the shape of the ZPE correction essentially is identical to the one of the corresponding plateau reaction of triazole and guanidine and thus the occurrence of an intermediate has only little impact on the ZPE contribution. Consequently, the hump in Figure 10 can easily be eliminated by proper substituents or solvent effects. However, due to the uncertainties associated with this aspect, we have restricted our discussion to the potential energy only.

6. Tunneling Effects

Tunneling effects are most relevant for proton-transfer reactions, as has been stressed by several authors.[5] Therefore, pure ab initio data for activation energies and rate constants without the consideration of tunneling corrections can serve as upper or lower bounds only. Since many approaches for computing tunneling corrections are restricted to a certain shape of the potential,[31,36,37] we derived a numerical method for calculating one-dimensional (1D) transmission probabilities of arbitrarily shaped potentials based on a generalization of the well-known model of a barrier with a finite height and width.[36] We note here that numerical approaches have been derived also by other authors.[38] To represent the reaction profile along the minimum energy path as accurately as possible, our 1D model makes use of N subsequent boxes (similar to a numerical integration scheme) with a constant width d. The height of each box is given by the profile. At the transition from one box to another (i.e., $s_n = nd$) we request continuity and differentiability of the wave function. Note that s is 0.0 for the geometry of the reactants. As is demonstrated in many textbooks,[36] for one box with constant height V_n the Schrödinger equation is solved at any point s of the reaction coordinate (without mass weighting) by

$$\Psi_n(s) = a_n e^{k_n s} + b_n e^{-k_n s} \quad \text{with} \quad k_n = \frac{1}{\hbar}\sqrt{2\mu(V_n - E)} \tag{5}$$

In this equation μ denotes the reduced mass and E is the total energy of the system. The coefficients a and b are those that need to be determined. Consequently, a generalization of this basic approach to N boxes yields two equations at the transition from box $n-1$ to the nth box:

$$a_{n-1}e^{k_{n-1}nd} + b_{n-1}e^{-k_{n-1}nd} = a_n e^{k_n nd} + b_n e^{-k_n nd} \tag{6}$$

$$k_{n-1}a_{n-1}e^{k_{n-1}nd} - k_{n-1}b_{n-1}e^{-k_{n-1}nd} = k_n a_n e^{k_n nd} + k_n b_n e^{-k_n nd} \tag{7}$$

These equations constitute an inhomogeneous system of $2N-2$ equations but $2N$ variables. Considering a stream of particles from the left, there is no reflection once the last box has been passed. As a consequence, b_N is zero. Moreover, the transmission probability is related to the ratio between the first (a_1) and the last coefficient (a_N) and thus one of these two coefficients can be set to 1. As a result, the linear set of equations is uniquely determined and can be solved by standard routines. The accuracy of this approach has been checked against the analytical solution (based on a linear combination of two hypergeometrical expansions) for the Eckart potential of the self-exchange reaction.[31] By use of the fit functions of the gauss-shaped Eckart-potential for representing the reaction profile, both approaches were found to yield identical results for the transmission probability.

On the basis of the model described above, the transmission probabilites of the autocatalytic self-exchange reaction A and the plateau reaction B have been computed with 200 intervals. Following the approach of Meyer and Günthard[39,40] a reduced mass μ given by

$$\frac{1}{\mu} = \sum_{i=1}^{N} m_i^{-1} \frac{\partial s}{\partial \mathbf{x}_i} \cdot \frac{\partial s}{\partial \mathbf{x}_i} \tag{8}$$

has been used throughout. In this equation m_i denotes the mass of atom i and $\mathbf{x}_i$ is its Cartesian coordinate vector. The variation of the reduced mass along the reaction path is shown in Figure 11 for both reactions. The general shape of these curves differs considerably and the reduced mass of the plateau reaction appears to be strongly influenced by different coordinates. This must be considered a result of the different reaction paths and the different molecular systems. The wiggles in the plot of the reduced mass of the plateau reaction are attributed to uncertainties in the reaction path in the region where the plateau is very flat. Deuteration of the N-atoms involved in the hydrogen bonds confirms the results discussed above that the outer regions of the reactions are dominated by coordinates other than those involving the hydrogen atoms. Moreover, for reaction B the edges of the plateau are clearly dominated by the proton transfers (i.e., the reduced mass is close to 1.0) while the center of the plateau is also characterized by other coordinates involving heavy atoms.

A plot of the CCSD(T) transmission probability dependence on the energy of the systems (relative to the barrier heights of the reactions) is provided in Figure 12. The difference between the two systems is easily seen. The curve of the plateau reaction is much closer to the classical limit (i.e., $P = 0.0$ for $E/V_{max} < 1.0$ and $P = 1.0$ for $E/V_{max} \geq 1.0$) than the corresponding curve of the autocatalytic reaction. Moreover, for the plateau reaction strong scattering resonances and nonclassical reflections can be observed, which have significant impact on the transmission coefficient κ. Transmission coefficients κ have been determined by numerical integration. At 330 K a transmission coefficient of 14.4 has been computed for the self-exchange reaction at the CCSD(T) level. VTST calculations, subsequently corrected by the transmission coefficient obtained from the numerical approach, yield a rate constant of 3690 s^{-1} for the self-exchange reaction. As mentioned above, energies were taken from CCSD-(T) calculations, while gradient and Hessian information refer to MP2 calculations. The obtained results are in excellent agreement with the experimental value of 6400 s^{-1} provided by de Paz et al.[8] The same holds true for the effective activation energy: our VTST/CCSD(T) value (corrected for tunneling contributions) of 43.6 kJ/mol closely resembles the experimental value reported by de Paz et al. (44.4 kJ/mol). Although the experimental data were obtained from solid-state measurements, they are in significantly better agreement with the computational data of this study rather than those obtained from unrelaxed geometries as reported by de Paz et al. This indicates that even in the solid state the molecules may fully relax during the reaction. On the other hand, relaxation were found to have significant impact on the energetics of the reaction.[8] For that reason, we consider reaction profiles for SPTR steps obtained from frozen geometry parameters less reliable than the partitioning scheme outlined above.

In contrast to the transmission coefficient of reaction A, which indicates nonnegligible tunneling effects, κ was computed to be 0.89 for the plateau reaction at the CCSD(T)/[aug]-cc-pVDZ level. This, of course, is an extraordinary result for a double proton transfer reaction. The result that κ was found to be smaller than 1.0 must be attributed to the nonclassical reflections

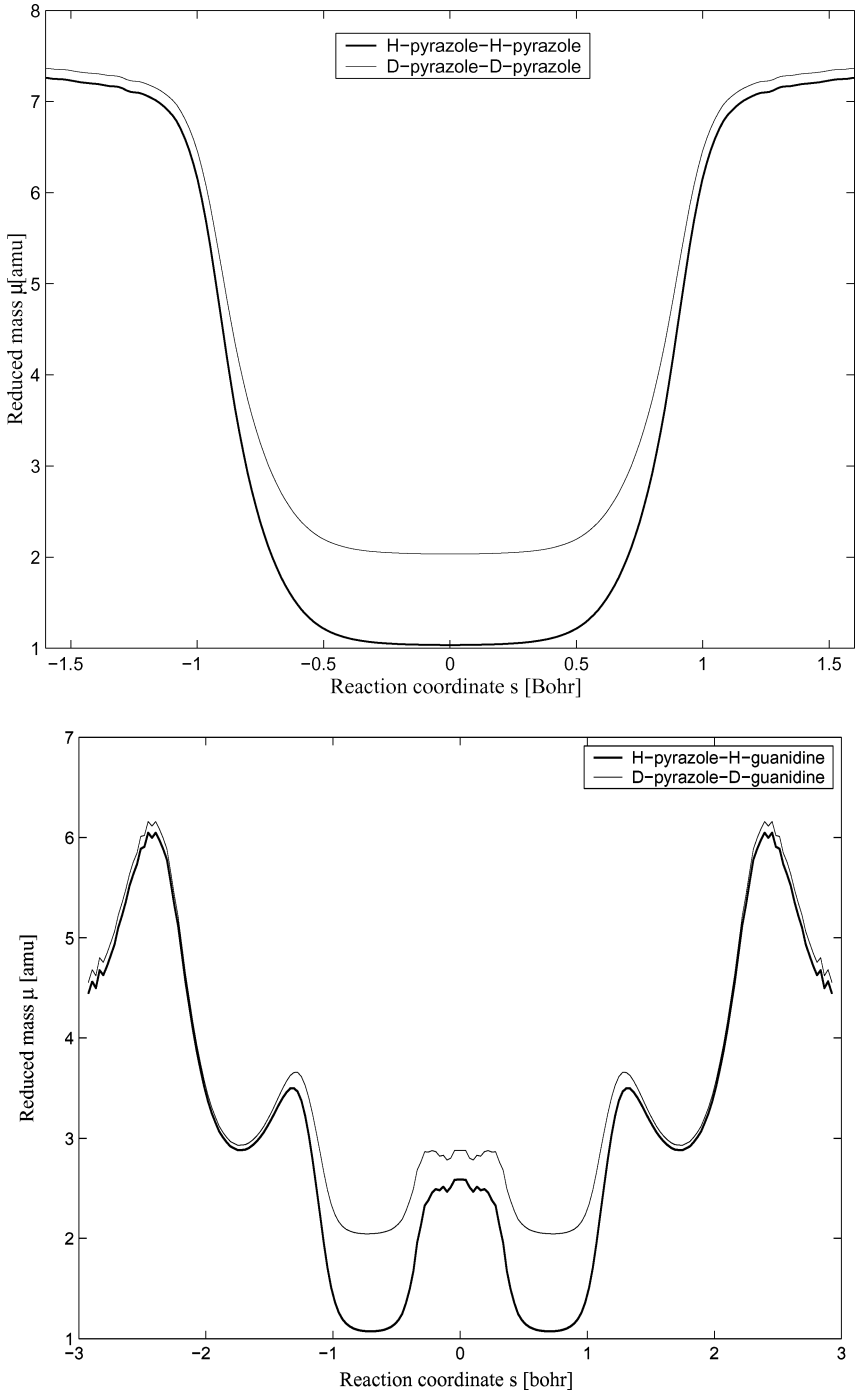

Figure 11. Variation of the reduced masses along the IRC of reactions A (upper plot) and B (lower plot).

that compensate for the tunneling effects at low energies. However, this value must still be considered with care since higher dimensional tunneling contributions (corner cutting effects) have been neglected due to the restriction of all trajectories to the 1D minimum energy path. A plot of the temperature dependence of the transmission coefficients is provided in Figure 13. This graph underlines the exceptional properties of plateau reactions.

The tunneling effects considered above refer to double proton tunneling. Double proton transfer reactions with separated potentials (i.e., with a reactive intermediate involved) give rise to single proton tunneling. For SPTRs, tunneling effects can be significant.[30] According to these considerations, transmission coefficients may be smallest for plateau reactions but rise for reaction profiles with separated or Eckart-type potentials.

Since the transmission coefficient enters into the equations for the rate constants, it has certain impact on kinetic isotope effects (KIE). We have estimated KIEs from simple transition-state theory (TST) according to

$$\ln\left(\frac{k_{HH}}{k_{DD}}\right) \approx \frac{1}{k_B T}(\Delta Z_{HH} - \Delta Z_{DD}) + \ln\left(\frac{\kappa_{HH}}{\kappa_{DD}}\right) \qquad (9)$$

where k_B denotes the Boltzmann constant, T is the temperature, k specifies the rate constant, and ΔZ is the ZPE difference between the structures of the reactants and the transition state. For the autocatalytic reaction A, k_{HH}/k_{DD} has been estimated from CCSD(T) calculations to be 12.9 (without tunneling correction) and 51.4 (including tunneling contributions) at $T =$ 330 K (frequencies have been scaled by 0.95 in order to account

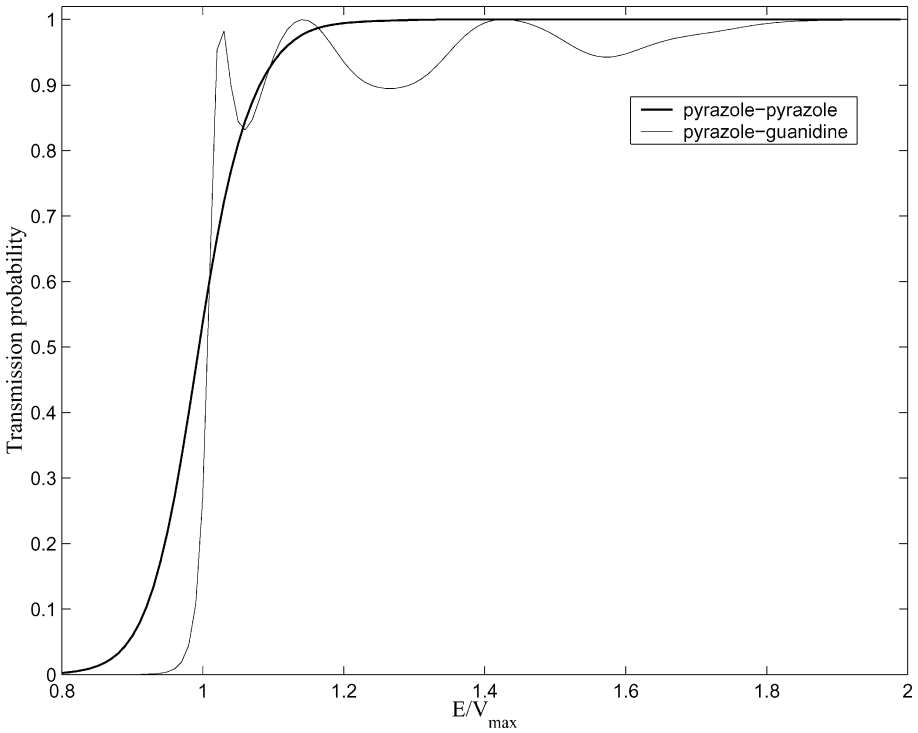

Figure 12. Comparison of the transmission probabilities of reactions A and B.

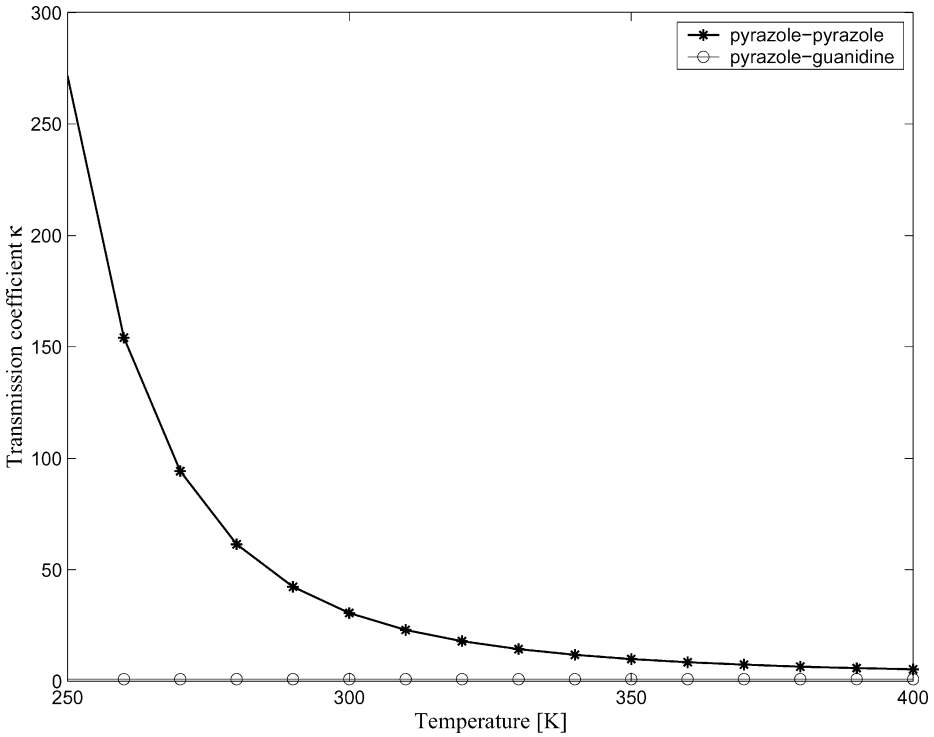

Figure 13. Comparison of the transmission coefficients of reactions A and B.

for anharmonicity corrections). The latter value is about twice as large as the experimental value of ca. 25 reported by de Paz et al.[8] We attribute this discrepancy mainly to the simple treatment of the tunneling contribution; more sophisticated models are currently under development. A proper choice for the ZPE at the transition state may be troublesome in the case of plateau reactions, because any point on top of the plateau may serve as the transition state. However, in the case considered here the formal transition state must be considered the point with the highest ZPE correction, which (according to Figure 10) coincides with the point at $s = 0.0$ amu$^{1/2}$·Bohr. Accordingly, the kinetic isotope effects for the plateau reaction have been computed at the same level of theory and were found to be significantly smaller, i.e., 3.2 and 3.4, respectively. This is in agreement with the general observation that kinetic isotope effects are considerably smaller for stepwise mechanisms than for synchronous ones.

7. Prediction of Plateau Reactions

The most prevalent question concerns the prediction of plateau reactions. As reported recently,[30] in a crude approximation it appears to be feasible to split the total interaction energy

between the monomers within the structure of the reactants into two contributions arising from the two hydrogen bonds. This has been accomplished by an empirical formula for the BSSE-corrected total interaction energy ΔE [as obtained from CCSD-(T) calculations; for further details see ref 30]:

$$\Delta E = A[e^{B(PA_1 - DE_2)} + e^{B(PA_2 - DE_1)}] \quad (10)$$

Herein, *PA* denotes the proton affinity and *DE* the deprotonation energy of monomers 1 and 2 as indicated by the subscript. *A* has been optimized by a least-squares procedure to 282.1 kJ/mol and *B* to 0.00374 mol/kJ. The first term of the equation can be attributed to one hydrogen bond, while the second term refers to the other. Consequently, the ratio of the two hydrogen bonds can be computed according to

$$r = e^{B[\Delta(PA) + \Delta(DE)]} \quad (11)$$

which is a function of monomeric properties only. $\Delta(PA)$ and $\Delta(DE)$ denote the differences between the proton affinities and the deprotonation energies. Using a data set of 17 complexes (mainly pyrazole and triazole derivatives bridged to guanidine and acetamidine molecules, all of them including nearly linear N−H hydrogen bonds only), we tried to correlate the ratio r with the nature of the reaction profile. According to our results, a ratio of $1 \leq r \leq 1.7$ characterizes an Eckart potential, while all plateau reactions were found in the range of $1.8 \leq r \leq 3.5$. For larger values of r the potential was split into two parts, separated by a zwitterionic intermediate. In addition, a neural network based on the proton affinities and deprotonation energies of the monomers has been used to predict the shape of the potential. It was found equally successful as the ratio r. As a result, it appears to be possible to predict plateau reactions from monomeric properties only. However, larger data sets and extensions to other hydrogen bonds rather than N−H are necessary to validate this criterion.

8. Conclusions

The DPTR of the pyrazole−guanidine system was found to be a plateau reaction with a structureless transition region of almost constant energy. In comparison with other proton transfer reactions, the system shows unusual properties, as has been demonstrated for tunneling effects and kinetic isotope effects. Therefore, plateau reactions are remarkable and require further investigations to come. In principle, plateau reaction must be considered the borderline case at the transition from synchronous to stepwise DPTRs. For the systems under investigation, electron correlation is substantial and requires computational methods beyond the MP2 level. One-dimensional tunneling effects were found to be negligible for this class of double proton-transfer reactions. Likewise, kinetic isotope effects are considerably smaller for these systems than for synchronous proton transfers. By use of empirical estimates, it appears to be feasible to predict plateau reactions from monomeric properties only.

Acknowledgment. Financial support by the Deutsche Forschungsgemeinschaft (RA 656/5-1) is kindly acknowledged. We thank Professor H. Stoll for many helpful discussions.

References and Notes

(1) Kratochvil, M.; Sponer, J.; Hobza, P. *J. Am. Chem. Soc.* **2000**, *122*, 3495.
(2) Smets, J.; Adamowicz, L.; Maes, G. *J. Phys. Chem.* **1996**, *100*, 6434.
(3) Chandra, A. K.; Nguyen, M. T.; Zeegers-Huyskens, T. *J. Mol. Struct. (THEOCHEM)* **2000**, *519*, 1.
(4) Alhambra, C.; Luque, F. J.; Gago, F.; Orozco, M. *J. Phys. Chem. B* **1997**, *101*, 10075.
(5) Loerting, T.; Liedl, K. R. *J. Am. Chem. Soc.* **1998**, *120*, 12595.
(6) Aguilar-Parrilla, F.; Scherer, G.; Limbach, H. H.; Foces-Foces, M. C.; Cano, F. H.; Smith, J. A. S.; Toiron, C.; Elguero, J. *J. Am. Chem. Soc.* **1992**, *114*, 9657.
(7) Smith, J. A. S.; Wehrle, B.; Aguilar-Parrilla, F.; Limbach, H. H.; Foces-Foces, M. C.; Cano, F. H.; Elguero, J.; Baldy, A.; Pierrot, M.; Khurshid, M. M. T.; Larcombe-McDouall, J. B. *J. Am. Chem. Soc.* **1989**, *111*, 7304.
(8) de Paz, J. L. G.; Elguero, J.; Foces-Foces, C.; Llamas-Saiz, A. L.; Aguilar-Parilla, F.; Klein, O.; Limbach, H. H. *J. Chem. Soc., Perkin Trans.* **1997**, *2*, 101.
(9) Douhal, A.; Guallar, V.; Moreno, M.; Lluch, J. M. *Chem. Phys. Lett.* **1996**, *256*, 370.
(10) Kim, Y.; Lim, S.; Kim, H. J.; Kim, Y. *J. Phys. Chem. A* **1999**, *103*, 617.
(11) Lim, J. H.; Lee, E. K.; Kim, Y. *J. Phys. Chem. A* **1997**, *101*, 2233.
(12) Bell, R. L.; Truong, T. N. *J. Phys. Chem. A* **1997**, *101*, 7802.
(13) Simperler, A.; Mikenda, W.; Schwarz, K. *Chem. Eur. J.* **2001**, *7*, 1606.
(14) Florian, J.; Hrouda, V.; Hobza, P. *J. Am. Chem. Soc.* **1994**, *116*, 1457.
(15) Peeters, D.; Leroy, G.; Wilante, C. *J. Mol. Struct.* **1997**, *416*, 21.
(16) Dunning, T. H. *J. Chem. Phys.* **1989**, *90*, 1007.
(17) Raghavachari, K.; Trucks, G. W.; Pople, J. A.; Head-Gordon, M. *Chem. Phys. Lett.* **1989**, *157*, 479.
(18) Møller, C.; Plesset, M. S. *Phys. Rev.* **1934**, *46*, 618.
(19) MOLPRO is a package of ab initio programs written by H.-J. Werner, and P. J. Knowles, with contributions from R. D. Amos, A. Berning, D. L. Cooper, M. J. O. Deegan, A. J. Dobbyn, F. Eckert, C. Hampel, T. Leininger, R. Lindh, A. W. Lloyd, W. Meyer, M. E. Mura, A. Nicklass, P. Palmieri, K. Peterson, R. Pitzer, P. Pulay, G. Rauhut, M. Schütz, H. Stoll, A. J. Stone, and T. Thorsteinsson; Version 2002.2; University of Birmingham, U.K., 1999 (see http://www.tc.bham.ac.uk/molpro/).
(20) Schmidt, M. W.; Baldridge, K. K.; Boatz, J. A.; Elbert, S. T.; Gordon, M. S.; Jensen, J. H.; Koseki, S.; Matsunaga, N.; Nguyen, K. A.; Su, S. J.; Windus, T. L.; Dupuis, M.; Montgomery, J. A. *J. Comput. Chem.* **1993**, *14*, 1347.
(21) Frisch, M. J.; Trucks, G. W.; Schlegel, H. B.; Scuseria, G. E.; Robb, M. A.; Cheeseman, J. R.; Zakrzewski, V. G.; Montgomery, J. A., Jr.; Stratmann, R. E.; Burant, J. C.; Dapprich, S.; Millam, J. M.; Daniels, A. D.; Kudin, K. N.; Strain, M. C.; Farkas, O.; Tomasi, J.; Barone, V.; Cossi, M.; Cammi, R.; Mennucci, B.; Pomelli, C.; Adamo, C.; Clifford, S.; Ochterski, J.; Petersson, G. A.; Ayala, P. Y.; Cui, Q.; Morokuma, K.; Malick, D. K.; Rabuck, A. D.; Raghavachari, K.; Foresman, J. B.; Cioslowski, J.; Ortiz, J. V.; Stefanov, B. B.; Liu, G.; Liashenko, A.; Piskorz, P.; Komaromi, I.; Gomperts, R.; Martin, R. L.; Fox, D. J.; Keith, T.; Al-Laham, M. A.; Peng, C. Y.; Nanayakkara, A.; Gonzalez, C.; Challacombe, M.; Gill, P. M. W.; Johnson, B. G.; Chen, W.; Wong, M. W.; Andres, J. L.; Head-Gordon, M.; Replogle, E. S.; Pople, J. A. *Gaussian 98*, revision A.1; Gaussian, Inc.: Pittsburgh, PA, 1998.
(22) Gonzalez, C.; Schlegel, H. B. *J. Chem. Phys.* **1989**, *90*, 2154.
(23) Gonzalez, C.; Schlegel, H. B. *J. Phys. Chem.* **1990**, *94*, 5523.
(24) Klamt, A.; Schüürman, G. *J. Chem. Soc., Perkin Trans.* **1993**, *2*, 799.
(25) Truhlar, D. G.; Garrett, B. C.; Klippenstein, S. J. *J. Phys. Chem.* **1996**, *100*, 12771.
(26) Truhlar, D. G. Direct Dynamics Methods for the Calculation of Reaction Rates. In *The Reaction Path in Chemistry*; Heidrich, D., Ed.; Kluwer: Dordrecht, The Netherlands, 1995; pp 229−256.
(27) Steckler, R.; Chuang, Y.-Y.; Fast, P. L.; Coitiño, E. L.; Corchado, J. C.; Hu, W.-P.; Liu, Y.-P.; Lynch, G. C.; Nguyen, K. A.; Jackels, C. F.; Gu, M. Z.; Rossi, I.; Clayton, S.; Melissas, V. S.; Garret, B. C.; Isaacson, A. D.; Truhlar, D. G. POLYRATE, Version 7.3; University of Minnesota: Minneapolis, MN, 1997.
(28) Corchado, J. C.; Coitino, E. L.; Chuang, Y.-Y.; Fast, P. L.; Truhlar, D. G. *J. Phys. Chem. A* **1998**, *102*, 2424.
(29) Boys, S. F.; Bernardi, F. *Mol. Phys.* **1970**, *19*, 553.
(30) Rauhut, G. *Phys. Chem. Chem. Phys.* **2003**, *5*, 791.
(31) Eckart, C. *Phys. Rev.* **1930**, *35*, 1303.
(32) Benderskii, V. A.; Makarov, D. E.; Wright, C. A. *Chemical Dynamics at Low Temperatures*; John Wiley & Sons: New York, 1994.
(33) Hammett, L. P. *J. Am. Chem. Soc.* **1937**, *59*, 96.
(34) Ritchie, C. D.; Sager, W. F. *Prog. Phys. Org. Chem.* **1964**, *2*, 323.
(35) Miller, W. H.; Handy, N. C.; Adams, J. E. *J. Chem. Phys.* **1980**, *72*, 99.
(36) Atkins, P. W.; Friedman, R. S. *Molecular Quantum Mechanics*; Oxford University Press: Oxford, U.K., 1997.
(37) Skodje, R. T.; Truhlar, D. G. *J. Phys. Chem.* **1981**, *85*, 624.
(38) Truhlar, D. G.; Kuppermann, A. *J. Am. Chem. Soc.* **1971**, *93*, 1840.
(39) Meyer, R.; Günthard, H. H. *J. Chem. Phys.* **1968**, *49*, 1510.
(40) Meyer, R.; Günthard, H. H. *J. Chem. Phys.* **1969**, *50*, 353.